Sensors and Materials, Vol. 35, No. 8 (2023) 2729–2740
MYU Tokyo

S & M 3350

Optical Properties of Nitride Cylindrical Quantum Dots as Biosensor Transducer

Dongmei Zheng,[1,2] Kun-Chieh Wang,[1*] Xiaofu Xu,[1,2] and Siyu Huang[1,2]

[1]School of Mechanical and Electrical Engineering, Sanming University, Sanming, Fujian Province 365004, China
[2]Key Laboratory of Intelligent Equipment of Fujian Higher Education Institute, Sanming University, Sanming, Fujian Province 365004, China

(Received April 7, 2023; accepted July 4, 2023)

Keywords: ZnSnN2, exciton, transition energy, oscillator strength, absorption coefficient

Nitride cylindrical quantum dots (NCQDs) are commonly used materials in optical chemical sensors and biosensors. We investigated the exciton-related optical properties of wurtzite $ZnSnN_2/In_xGa_{1-x}N$ cylindrical quantum dots (CQDs) with finite potential barriers. The energy states in a CQD system were computed by a variational scheme using the single-band effective mass approximation, which considers the effect of the built-in electric field (BEF). The results are presented in the form of a specific function of CQD structural parameters including height, radius, and In concentration in the barrier. Our major findings are as follows. First, the excitonic transition energy decreases with increasing CQD size and increases with increasing In concentration. Second, the oscillator strength rapidly decreases with increasing CQD height and slowly increases with increasing CQD radius. Furthermore, we obtained the absorption coefficient (AC) of the exciton as a function of the incident photon energy for different CQD structural parameters. We concluded that, in general, increasing any of the aforementioned structural parameters causes either a blueshift or redshift of the AC peak. A similar phenomenon occurs for the resonant peak intensity. In particular, a strong BEF leads to a redshift of the resonant peak and a decrease in its intensity.

1. Introduction

Nitride cylindrical quantum dots (NCQDs) are commonly used materials in optical chemical sensors and biosensors. Maier *et al.*(1) reported an optical chemical sensor that adopts nitride nanowire heterostructures grown by plasma-assisted molecular beam epitaxy on Si (111) substrates. Nötzel(2) reported an enzymatic biosensor for the detection of glucose and cholesterol for medical diagnostics that uses quantum dots (QDs) grown by plasma-assisted molecular beam epitaxy on a Si (111) substrate. Such nanomaterial-based semiconductor QD biosensors use optical readout schemes based on the luminescence properties of the QDs. He also found that, compared with optical and other sensing techniques, the nitride QD enzymatic electrochemical biosensors have excellent linearity, sensitivity, response time, stability, repeatability, reproducibility, and selectivity. Further, among the various materials frequently used for

*Corresponding author: e-mail: m18316252102@126.com
https://doi.org/10.18494/SAM4449

ISSN 0914-4935

NCQDs, wurtzite (WZ) $ZnSnN_2/In_xGa_{1-x}N$ cylindrical quantum dots (CQDs) with finite potential barriers are especially important as sensor materials because of their superior optical characteristics.

Research on the structural properties of Zn-IV-N_2 compounds (IV = Si, Ge, Sn) has been drawing much attention.[3–7] The crystal structure of a Zn-IV-N_2 compound is derived from the WZ III-nitride, where the group III ions are replaced by alternating Zn and group IV ions. By adding Si and Ge, the direct band gaps of Zn-(Si,Ge,Sn)-N_2 alloys may cover the entire visible light spectrum.[8,9] This feature gives Zn-(Si,Ge,Sn)-N_2 alloys promising performance for full-spectrum LED applications.[10–14] In addition, II-IV-N_2 compounds, which are closely related to the WZ-structured III-N semiconductors, have similar electronic and optical properties to InGaN, such as direct band gaps and large optical absorption coefficients.[9,15] Moreover, Zn and the IV group elements of Si and Sn are earth abundant and environment friendly.[16] Among the II-IV-N_2 materials, $ZnSnN_2$ is considered one of the most promising absorber materials in photovoltaic solar cell applications due to its excellent characteristics of an ideal solar-matched band gap, robust optical absorption, and low cost.[17–21] However, $ZnSnN_2$ is one of the least studied Zn-IV-N_2 compounds.

Computational research on the properties of $ZnSnN_2$ did not begin until 2008,[3] and the first synthesis of $ZnSnN_2$ was not reported until 2013.[15] Although extensive studies on this material are now under way, its basic electronic and optical properties have not yet been fully elucidated. Because the lattice constant of $ZnSnN_2$ is between those of GaN and InN, it can be lattice-matched to that of InGaN. Wang *et al.*[12] reported that the conduction band minimum of $ZnSnN_2$ is 1.44 eV lower than that of GaN and that the valence band maximum of $ZnSnN_2$ is 0.39 eV higher than that of GaN.[22] Therefore, a $ZnSnN_2$ layer may serve as a well layer in the heterostructure system of $ZnSnN_2/In_xGa_{1-x}N$, in which x may reach up to 0.5. Several possible applications of $ZnSnN_2/In_xGa_{1-x}N$ quantum wells (QWs) in optoelectronics and electronics have been investigated, such as the use of InGaN-$ZnSnN_2$ QWs for high-efficiency amber LEDs,[12] an LED tunable in the IR range that is based on InGaN-$ZnSnN_2$/GaN QWs,[13] and QW-based near-IR LEDs.[14] Moreover, in a WZ $In_xGa_{1-x}N/ZnSnN_2/In_xGa_{1-x}N$ QW structure with the c axis parallel to the growth direction, a piezoelectric (PE) field may occur in the $ZnSnN_2$ due to its lattice mismatch with $In_xGa_{1-x}N$, and a sizeable local surface plasmon (SP) resonance across the $ZnSnN_2$ layer also appears. The total built-in electric field (BEF) is estimated to have an order of magnitude of MV/cm and to decrease as the In concentration x increases.[23] Hence, the optical properties of [0001]-oriented WZ $ZnSnN_2/In_xGa_{1-x}N$ strained QWs are strongly affected by the BEF.

Although the optical properties of III-V nitride QDs have been fully studied, WZ $ZnSnN_2/In_xGa_{1-x}N$ QDs have not yet been fully analyzed. Thus, as reported in this paper, we have theoretically studied the excitonic transition energy, the oscillator strength, and the effect of the BEF in a WZ $ZnSnN_2/In_xGa_{1-x}N$ CQD with geometrical confinement. In numerical calculations, we use a variational scheme with a single-band effective mass approximation. We also fully investigated the absorption coefficient (AC) of the exciton as a function of the incident photon energy (IPE) for different CQD structural parameters (height, radius, and In concentration in the barrier).

2. Theoretical Foundation

In accordance with previous theoretical studies on WZ semiconductor QDs,[24–26] we now consider a $ZnSnN_2$ CQD with height L along the c axis and radius R embedded in an $In_xGa_{1-x}N$ barrier material (Fig. 1). On the basis of the single-band effective mass approximation,[24] the Hamiltonian of an exciton confined in a $ZnSnN_2/In_xGa_{1-x}N$ CQD is given by

$$\hat{H}_{\mathrm{ex}} = H_{\mathrm{e}} + H_{\mathrm{h}} + E_{\mathrm{g,ZnSnN_2}} - \frac{e^2}{4\pi\varepsilon_0\bar{\varepsilon}\left|\vec{r}_{\mathrm{e}} - \vec{r}_{\mathrm{h}}\right|}, \tag{1}$$

where $\hat{H}_j$ (j = e or h) can be written as

$$\hat{H}_{\mathrm{e}} = -\frac{\hbar^2}{2m^*_{\mathrm{e}\perp}}\left[\frac{1}{\rho_{\mathrm{e}}}\frac{\partial}{\partial\rho_{\mathrm{e}}}\left(\rho_{\mathrm{e}}\frac{\partial}{\partial\rho_{\mathrm{e}}}\right) + \frac{1}{\rho_{\mathrm{e}}^2}\frac{\partial^2}{\partial\phi_{\mathrm{e}}^2}\right] - \frac{\hbar^2}{2m^*_{\mathrm{e}//}}\frac{\partial^2}{\partial z_{\mathrm{e}}^2} + V(\rho_{\mathrm{e}}) + V(z_{\mathrm{e}}) - eFz_{\mathrm{e}} \tag{2}$$

and

$$\hat{H}_{\mathrm{h}} = -\frac{\hbar^2}{2m^*_{\mathrm{h}\perp}}\left[\frac{1}{\rho_{\mathrm{h}}}\frac{\partial}{\partial\rho_{\mathrm{h}}}\left(\rho_{\mathrm{h}}\frac{\partial}{\partial\rho_{\mathrm{h}}}\right) + \frac{1}{\rho_{\mathrm{h}}^2}\frac{\partial^2}{\partial\phi_{\mathrm{h}}^2}\right] - \frac{\hbar^2}{2m^*_{\mathrm{h}//}}\frac{\partial^2}{\partial z_{\mathrm{h}}^2} + V(\rho_{\mathrm{h}}) + V(z_{\mathrm{h}}) + eFz_{\mathrm{h}}. \tag{3}$$

All symbols in the above equations are described in Refs. 25 and 26. F is the BEF and can be calculated as[25,26]

$$F = \begin{cases} \left|-\dfrac{P_{\mathrm{SP}}^{\mathrm{ZnSnN_2}} + P_{\mathrm{PE}}^{\mathrm{ZnSnN_2}} - P_{\mathrm{SP}}^{\mathrm{In_xGa_{1-x}N}}}{\varepsilon_{\mathrm{e}}^{\mathrm{ZnSnN_2}}\varepsilon_0}\right|, & \left|z_{\mathrm{e}}\text{or } z_{\mathrm{h}}\right| \le \dfrac{L}{2}, \rho \le R \\ 0, & \left|z_{\mathrm{e}}\text{or } z_{\mathrm{h}}\right| > \dfrac{L}{2}, \rho > R \end{cases}, \tag{4}$$

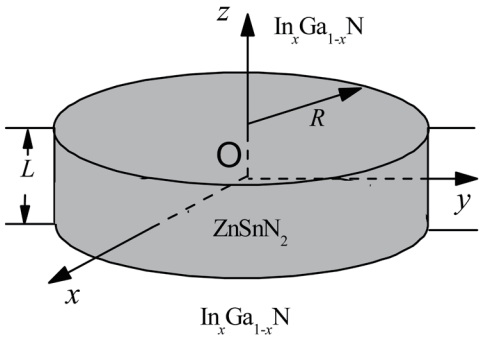

Fig. 1. Diagram of the $ZnSnN_2$ CQD structure with radius R and height L surrounded by $In_xGa_{1-x}N$ in both the radial and z directions.

where $P_{PE}(P_{SP})$ is the PE (spontaneous) polarization and $\varepsilon_e^{ZnSnN_2}$ is the electronic dielectric constant of $ZnSnN_2$.

In Eqs. (2) and (3), $V(\rho_j)$ and $V(z_j)$ are, respectively, the in-plane and z-direction confinement potentials of the electron (hole) in the WZ $ZnSnN_2/In_xGa_{1-x}N$ CQD structure. These parameters can be calculated via

$$V(\rho_j)=\begin{cases}0, & \rho_j \le R\\ Q_j[E_{g,\mathrm{In}_x\mathrm{Ga}_{1-x}\mathrm{N}}-E_{g,\mathrm{ZnSnN}_2}], & \rho_j > R\end{cases} \tag{5}$$

and

$$V(z_j)=\begin{cases}0, & |z_j|\le \dfrac{L}{2}\\ Q_j[E_{g,\mathrm{In}_x\mathrm{Ga}_{1-x}\mathrm{N}}-E_{g,\mathrm{ZnSnN}_2}], & |z_j|> \dfrac{L}{2}\end{cases}, \tag{6}$$

where Q_j is the band offset ratio, taken as 79.5:20.5 for both the conduction band and the valence band.[22]

The eigenfunction of the Hamiltonians $\hat{H}_j$ can be written in the form[24–26]

$$\psi_j(\rho_j,\phi_j,z_j)=f(\rho_j)h(z_j)e^{im\phi_j}, \quad m=0,\ \pm1,\ \pm2,\ldots. \tag{7}$$

The time-independent Schrödinger equation for this exciton system is given by

$$\hat{H}_{ex}\Phi_{ex}(\vec{r}_e,\vec{r}_h)=E_{ex}\Phi_{ex}(\vec{r}_e,\vec{r}_h), \tag{8}$$

where E_{ex} is the eigenenergy and $\Phi_{ex}(\vec{r}_e,\vec{r}_h)$ is the eigenfunction. To find the eigenenergy, in the variation we choose the trial wave function[24–26]

$$\Phi_{ex}(\vec{r}_e,\vec{r}_h)=\psi_e(\rho_e,\phi_e,z_e)\psi_h(\rho_h,\phi_h,z_h)e^{-\alpha\rho_{eh}^2}e^{-\beta z_{eh}^2}. \tag{9}$$

The ground-state energy E_{ex} is defined as

$$E_{ex}=\min_{\alpha,\beta}\frac{\left\langle\Phi_{ex}(\vec{r}_e,\vec{r}_h)\middle|\hat{H}_{ex}\middle|\Phi_{ex}(\vec{r}_e,\vec{r}_h)\right\rangle}{\left\langle\Phi_{ex}(\vec{r}_e,\vec{r}_h)\middle|\Phi_{ex}(\vec{r}_e,\vec{r}_h)\right\rangle}. \tag{10}$$

The binding energy E_b and interband transition energy E_{ph} can be calculated as[24,25]

$$E_{\mathrm{b}} = E_{\mathrm{e}} + E_{\mathrm{h}} + E_{g,\mathrm{ZnSnN_2}} - E_{\mathrm{ex}} \tag{11}$$

and

$$E_{\mathrm{ph}} = E_{\mathrm{e}} + E_{\mathrm{h}} + E_{g,\mathrm{ZnSnN_2}} - E_{\mathrm{b}}\,, \tag{12}$$

where $E_{\mathrm{e}} + E_{\mathrm{h}}$ is the summation of the free electron and hole confinement energies in the same CQD.

The oscillator strength f_{ex} for the exciton ground state can be computed as[27,28]

$$f_{\mathrm{ex}} = \frac{2P^2}{m_0 E_{\mathrm{ex}}} \frac{\left| \int d\vec{r}_{\mathrm{e}} d\vec{r}_{\mathrm{h}} \Phi_{\mathrm{ex}}(\vec{r}_{\mathrm{e}}, \vec{r}_{\mathrm{h}}) \delta(\vec{r}_{\mathrm{e}} - \vec{r}_{\mathrm{h}}) \right|^2}{\left\langle \Phi_{\mathrm{ex}}(\vec{r}_{\mathrm{e}}, \vec{r}_{\mathrm{h}}) \middle| \Phi_{\mathrm{ex}}(\vec{r}_{\mathrm{e}}, \vec{r}_{\mathrm{h}}) \right\rangle}\,. \tag{13}$$

In the calculation, we set $P^2/m_0 = 1$ eV.[28]

The AC is given by[26]

$$\alpha(\hbar\omega) = \frac{\pi e^2 P^2}{3nc\varepsilon_0 m_0^2 \omega V} \frac{\left| \int d\vec{r}_{\mathrm{e}} d\vec{r}_{\mathrm{h}} \Phi_{\mathrm{ex}}(\vec{r}_{\mathrm{e}}, \vec{r}_{\mathrm{h}}) \delta(\vec{r}_{\mathrm{e}} - \vec{r}_{\mathrm{h}}) \right|^2}{\left\langle \Phi_{\mathrm{ex}}(\vec{r}_{\mathrm{e}}, \vec{r}_{\mathrm{h}}) \middle| \Phi_{\mathrm{ex}}(\vec{r}_{\mathrm{e}}, \vec{r}_{\mathrm{h}}) \right\rangle} \times \delta(E_{\mathrm{ph}} - \hbar\omega) \tag{14}$$

and

$$\delta(E_{\mathrm{ph}} - \hbar\omega) = \frac{\Gamma}{\pi[(E_{\mathrm{ph}} - \hbar\omega)^2 + \Gamma^2]}\,, \tag{15}$$

where V and $\hbar\omega$ represent the sample volume and the IPE, respectively. Γ is the line width of the exciton, and in our calculation, we set $\Gamma = 5$ meV.[29]

3. Results and Discussion

Through calculations using the above equations, we obtain the excitonic transition energy and the oscillator strength as functions of the QD structural parameters in the strained WZ $ZnSnN_2/In_{0.2}Ga_{0.8}N$ CQD. In addition, the AC is investigated for different QD structural parameters. The material parameters are given in Table 1. All the material parameters of $In_xGa_{1-x}N$, are computed through linear interpolation, except for E_{g}. The bowing parameter of the band gap for $In_xGa_{1-x}N$ is set as 3.2 eV.[22]

Table 1
Material parameters of ZnSnN2, GaN, and InN. Data obtained from Refs. 9, 14, and 23 ($ZnSnN_2$) and Refs. 30 and 31 (GaN and InN).

Parameter	Symbol	$ZnSnN_2$	GaN	InN
Band energy (eV)	E_g	1.8	3.507	1.994
Lattice constant (nm)	α	0.338	0.3189	0.3545
PE constant (C/m^2)	e_{31}	−0.59	—	—
	e_{33}	1.09	—	—
Elastic constant (GPa)	C_{13}	100	—	—
	C_{33}	306	—	—
Static dielectric constant	ε	15.088	—	—
Electronic effective mass (m_0)	$m_e^{\parallel}$	0.12	0.2	0.12
	$m_e^{\perp}$	0.16	0.2	0.12
Effective mass of hole (m_0)	$m_h^{\parallel}$	2.04	1.10	1.61
	$m_h^{\perp}$	2.02	1.65	1.67
Electronic dielectric constant	ε_e	5.7		
Spontaneous polarization (C/m^2)	P_{sp}	−0.029	−0.029	−0.032

3.1 Variation of excitonic transition energy

Figure 2 shows the calculated variation of E_{ph} as a function of the CQD size in the $ZnSnN_2$/$In_{0.2}Ga_{0.8}N$ CQD. E_{ph} decreases as L or R increases and drops below the bulk WZ $ZnSnN_2$ energy gap when L is higher than 3.5 nm for all radii of the CQD. This is because the confined energies of the electron and hole decrease with increasing CQD size. In addition, L has a more pronounced influence than R on E_{ph} because the BEF in the $ZnSnN_2$ layer is along the growth direction of the heterostructure, and it may affect E_{ph} via the quantum-confined Stark effect. The variation predicted using our proposed formula, which adopts the optical transition energy as a function of the CQD size, closely matches those of the InGaN/GaN CQD reported by Shi and Gan[24] and the GaN/AlGaN QD reported by Minimala *et al.*[27]

We now investigate the variation of the excitonic transition energy E_{ph} as a function of the In concentration x of WZ $ZnSnN_2/In_xGa_{1-x}N$ CQDs with L = 3 nm and R = 6 nm. Figure 3 shows that E_{ph} is significantly influenced by the BEF, also increasing with increasing x. In contrast, without the BEF, E_{ph} decreases with increasing In concentration x. The reason for this phenomenon is as follows. When the BEF originating from SP and PE polarizations in the Hamiltonian is included, the In concentration in the barrier affects E_{ph} by both decreasing the confined potential of the electron and hole and decreasing the BEF. Increasing the In concentration x results in (i) a decrease in the electron and hole confined energies because a decrease in the potential barrier height leads to a redshift of E_{ph}, and (ii) a decrease in the BEF because of the occurrence of a blueshifted energy spectrum. The latter result dominates in the case of $ZnSnN_2/In_xGa_{1-x}N$ CQDs with L = 3 nm; thus, E_{ph} exhibits a redshift with decreasing x. However, when the BEF is ignored, only the first result occurs with increasing x; therefore, E_{ph} decreases with increasing x. Moreover, Fig. 3 also clearly indicates that a strong BEF gives rise to a large decrease in E_{ph}, especially for QDs with low x.

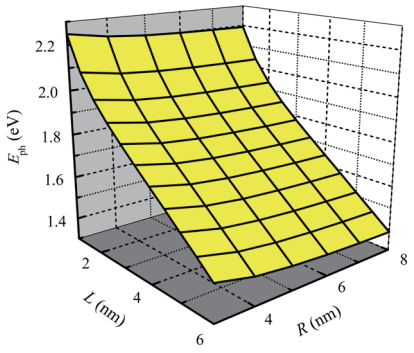

Fig. 2. (Color online) Variation of E_{ph} as a function of dot size in $ZnSnN_2/In_{0.2}Ga_{0.8}N$ CQD.

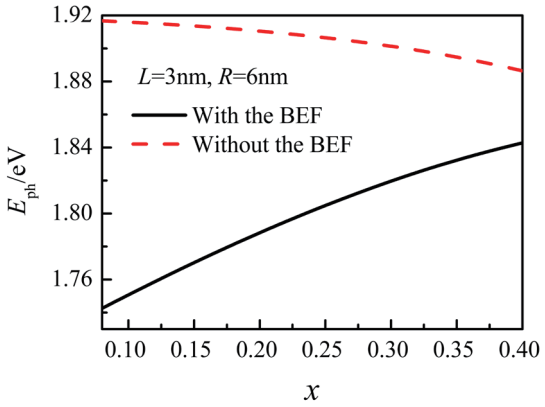

Fig. 3. (Color online) Variation of E_{ph} as a function of In concentration x in $ZnSnN_2/In_xGa_{1-x}N$ CQDs with L = 3 and R = 6 nm.

3.2 Oscillator strength

Figure 4 shows the obtained variation of the oscillator strength f_{ex} for the ground exciton state with the dot size in the $ZnSnN_2/In_{0.2}Ga_{0.8}N$ CQD. f_{ex} decreases rapidly with increasing CQD height L, approaching zero when L is near to 5.5 nm. The reason for this is as follows. f_{ex} is inversely proportional to E_{ex} and directly proportional to the square of the overlap integral between the electron and hole wave functions [see Eq. (13)]. As L increases, the electron–hole spatial separation in the z direction becomes large, which leads to an apparent reduction in the overlap integral between the electron and hole wave functions, and E_{ex} simultaneously decreases. However, the overlap integral between the electron and hole wave functions decreases by a larger margin than E_{ex}. Therefore, f_{ex} decreases rapidly with increasing L. Moreover, Fig. 4 illustrates that f_{ex} increases slowly with increasing R. The main reason for this is that the overlap integral increases as R increases, directly leading to an increase in the oscillator strength f_{ex}. Figure 4 further shows that the influence of L on f_{ex} is more visible than that of R because the BEF in the $ZnSnN_2$ layer is along the growth direction of the heterostructure. The predicted variation using our proposed formula, which adopts f_{ex} as a function of the QD size, is similar to that of the ZnO/MgZnO QD reported by Zheng *et al.*[26]

3.3 Variation of AC α

We next obtain the variation of the AC α as a function of the IPE $\hbar\omega$ with and without the BEF in the $ZnSnN_2/In_{0.2}Ga_{0.8}N$ QDs with R = 6 nm and different dot heights, as shown in Fig. 5. It is observed that the position of the peak of the AC α gradually shifts to the region where a lower photon energy occurs as L increases. Eventually, the AC peak value is obtained at the specific IPE that $\hbar\omega \approx E_{ph}$ [see Eqs. (14) and (15)]. The reason for this is as follows. As L increases, the excitonic transition energy decreases. As a result, the AC α peak exhibits a redshift with increasing L. Further, the AC peak intensity decreases as L increases. This is because the

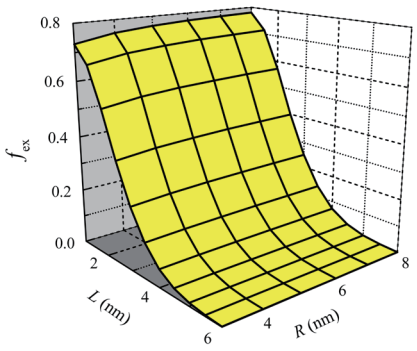

Fig. 4. (Color online) Variation of f_{ex} as a function of dot size in WZ $ZnSnN_2/In_{0.2}Ga_{0.8}N$ CQD.

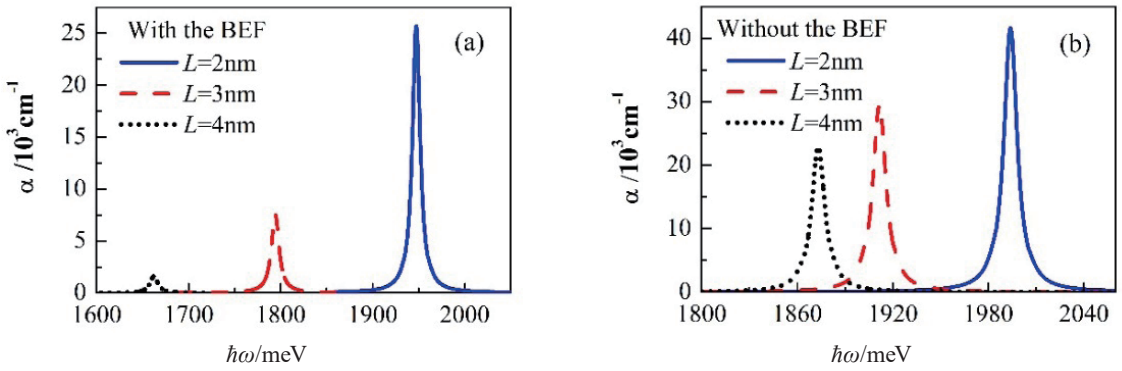

Fig. 5. (Color online) Variation of AC α with the IPE $\hbar\omega$ in $ZnSnN_2/In_{0.2}Ga_{0.8}N$ CQDs with R = 6 nm and different dot heights: (a) with the BEF effect and (b) without the BEF effect.

AC α is directly proportional to the square of the overlap integral between the electron and hole wave functions and inversely proportional to the sample volume [see Eq. (14)]. On the one hand, the sample volume increases with increasing L. On the other hand, as L increases, the quantum confinement attenuates, resulting in a decrease in the overlap of the electron and hole. Therefore, the AC peak intensity decreases with increasing CQD height L. Furthermore, comparing Figs. 5(a) and 5(b), we find that the magnitude of the AC α decreases and its peak is obtained at a lower IPE when the BEF in the Hamiltonian is included for a given CQD height L. For example, for L = 2 nm, when considering the BEF effect, the peak value of the AC α is 2.570 × 10^4 cm^{-1} and appears at an IPE of 1947.4 meV, whereas ignoring the BEF effect, the peak value of the AC α is about 4.163 × 10^4 cm^{-1} and appears at $\hbar\omega$ = 1994.0 meV. The difference in the peak AC values between the cases with and without the BEF effect is about 1.593 × 10^4 cm^{-1}, and the position of the AC peak for these two cases has a redshift difference of 46.6 meV. For L = 4 nm, the peak value of the AC α is 1.624 × 10^3 cm^{-1} (2.286 × 10^4 cm^{-1}) and appears at $\hbar\omega$ = 1662.2 (1873.2) meV with (without) the BEF effect. The difference in the peak AC intensity values between the cases with and without the BEF effect is about 2.124 × 10^4 cm^{-1}, and the position of the AC peak for these two cases has a redshift difference of 211.0 meV. These results

further illustrate the phenomenon that the influence of the BEF becomes significant with increasing QD height L. This is because the spatial separation of electrons and holes induced by the huge on-axis BEF in the WZ $ZnSnN_2/In_{0.2}Ga_{0.8}N$ heterostructure reduces their overlap. Thus, stronger BEFs reduce the intensity of the absorption peak. Moreover, it is known that the existence of BEFs always reduces the excitonic transition energy. Therefore, strong BEFs cause a redshift of the AC peak. The predicted variation using our proposed formula, which adopts the AC as a function of the CQD height, is similar to that of the ZnO/MgZnO CQD reported by Zheng *et al.*[26]

Considering the BEF effect, we now calculate the AC α as a function of the IPE $\hbar\omega$ in $ZnSnN_2/In_{0.2}Ga_{0.8}N$ CQDs with a height L of 3 nm and different radii R. The calculation result is shown in Fig. 6. As R increases, the AC peak moves towards a lower IPE accompanied by an apparent decrease in its intensity. For example, the AC peak intensity decreases from about 2.834×10^4 cm^{-1} for R = 3 nm to 1.078×10^4 cm^{-1} for R = 5 nm, and the AC peak undergoes a redshift from 1852.8 meV for R = 3 nm to 1802.8 meV for R = 5 nm. In addition, comparing Fig. 5(a) with Fig. 6 indicates that L exhibits a stronger influence than R on the AC α. Thus, our investigation of the exciton-related optical properties reveals that both the BEF and the QD height L play crucial roles.

Using Eqs. (14) and (15), we calculate the AC α as a function of the IPE $\hbar\omega$ with and without the BEF effect in $ZnSnN_2/In_xGa_{1-x}N$ CQDs with L = 3 nm and R = 6 nm for In concentrations of x = 0.1, 0.2, and 0.3, and the obtained result is shown in Fig. 7. When the BEF is included in the Hamiltonian, the AC peak gradually moves to the region where a high photon energy occurs, and the AC peak intensity increases with increasing In concentration. However, when the BEF is ignored, the AC peak shifts towards the region of low photon energy with increasing In concentration, whereas the intensity of the AC peak is insensitive to the In concentration in the barrier. The reason for this is as follows. The AC peak value is obtained where the IPE $\hbar\omega \approx E_{ph}$. From Fig. 3, we observe that the excitonic transition energy E_{ph} increases (decreases) with increasing In concentration x when the BEF effect is included (ignored). As a result, the AC peak with (without) the BEF effect undergoes a blueshift (redshift) with increasing In concentration.

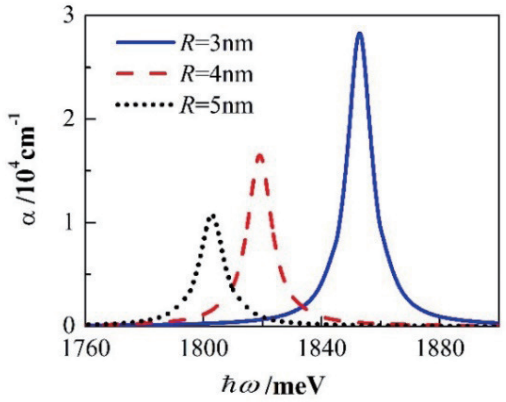

Fig. 6. (Color online) Variation of AC α with the IPE $\hbar\omega$ in $ZnSnN_2/In_{0.2}Ga_{0.8}N$ CQDs with L = 3 nm and different dot radii R.

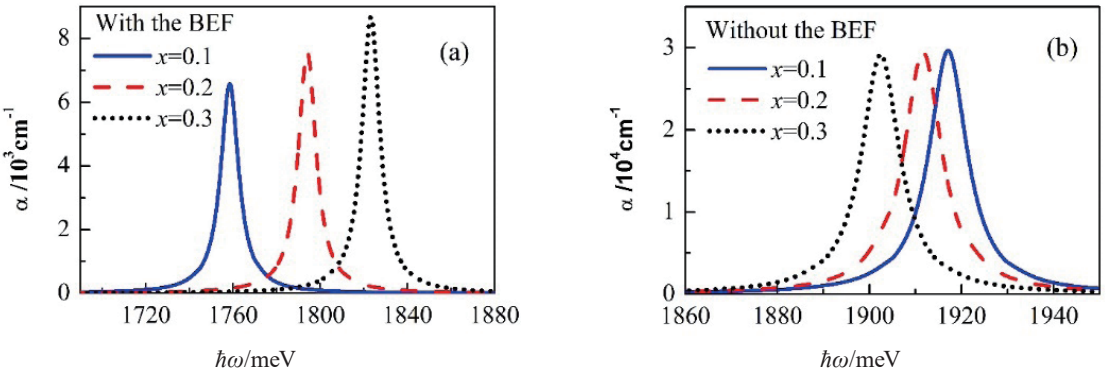

Fig. 7. (Color online) Variation of AC α with the IPE $\hbar\omega$ in $ZnSnN_2/In_{0.2}Ga_{0.8}N$ CQDs with $L = 3$ and $R = 6$ nm for In concentrations of $x = 0.1$, 0.2, and 0.3: (a) with the BEF effect and (b) without the BEF effect.

Furthermore, the intensity of the BEF in the strained $ZnSnN_2$ layer is weakened with increasing x, which enhances the overlap integral between the electron and hole wave functions. Hence, the absorption peak intensity is enhanced with increasing In concentration.

4. Conclusion

Determining the key factors affecting the optical properties of WZ $ZnSnN_2/In_xGa_{1-x}N$ CQDs with finite potential barriers is important for enhancing the sensing performance of biosensors or optical chemical sensors employing this material. In this study, considering the inclusion of a strong BEF due to SP and PE polarizations, we theoretically studied some of the optical properties of the exciton confined in WZ $ZnSnN_2/In_xGa_{1-x}N$ CQDs with finite potential barriers at all surfaces using a single-band effective mass approximation with the variational method. We calculated the transition energy as functions of the CQD structural parameters, including the CQD height L and radius R, and the In concentration x in the barrier layer. We also investigated the relationship between the oscillator strength and the CQD size. In addition, the calculated exciton states were used to evaluate the related AC as functions of the IPE for different CQD structure parameters. The main findings are as follows. The transition energy increases with decreasing CQD size and decreases with decreasing In concentration. The oscillator strength rapidly decreases with increasing CQD height and slowly increases with increasing CQD radius. Furthermore, the AC resonant peak undergoes a redshift (blueshift) as the CQD size or In concentration is increased with a decrease (an increase) in the resonant peak intensity. Moreover, we computed the AC of the exciton as a function of the IPE for different CQD structure parameters in cases with and without the BEF effect. We found that a strong BEF causes a redshift of the AC peak and dramatically decreases the resonant peak intensity. Therefore, to obtain a large AC, the adverse effects of the BEF should be minimized and the dot size should be modified. Although experimental results for exciton states and interband transitions in the WZ $ZnSnN_2/In_xGa_{1-x}N$ QD are still lacking, our obtained theoretical results will be useful for related physics experiments and for the design of some LEDs covering the visible light spectrum and photovoltaic solar cells based on WZ $ZnSnN_2/In_xGa_{1-x}N$ QD structures.

Acknowledgments

This work was supported by the Key Project of the Natural Science Foundation of the Education Department of Fujian Province (JZ160476), Natural Science Foundation of Fujian Province of China (2020J01387), Major Project of Sanming Science and Technology Plan (2019-G-7), Project of the Department of Science and Technology of Fujian Province, China (2021G02013, 2020H0049, 2021H0060), and in part by Sanming University of Fujian Province, China (19YG05, 19YG04) and Incubation Program of the National Science Foundation of China from Sanming University (PYT2108).

References

1 K. Maier, A. Helwig, G. Müller, P. Becker, P. Hille, J. Schörmann, J. Teubert, and M. Eickhoff: Sens. Actuators, B **197** (2014) 87. https://doi.org/10.1016/j.snb.2014.02.002
2 R. Nötzel: Nation. Sci. Rev. **4** (2017) 184. https://doi.org/10.1093/nsr/nww101
3 T. R. Paudel and W. R. L. Lambrecht: Phys. Rev. B **78** (2008) 115204. https://doi.org/10.1103/PhysRevB.78.115204
4 O. Masako, H. Dan, M. P. Monika, S. J. Laura, S. R. Stefan, S. Wolfgang, and E. Hubert: Phys. Rev. Mater. **5** (2021) 024601. https://doi.org/10.1103/PhysRevMaterials.5:024601
5 K. K. Chinnakutti, V. Panneerselvam, and S. T. Salammal: J. Alloy Compd. **885** (2021) 157380. https://doi.org/10.1016/j.jallcom.2020.157380
6 F. Ye, Q. Q. Chen, X, M. Cai, Y. Z. Xie, X. F. Ma, K. Vaithinathan, D. P. Zhang, P. Fana, and V. A. L. Roy: J. Mater. Chem. C **8** (2020) 4314. https://doi.org/10.1039/C9TC06965H
7 N. L. Adamski, D. Wickramaratne, and C. G. Van de Walle: J. Mate. Chem. C **8** (2020) 7890. https://doi.org/10.1039/D0TC01578D
8 P. C. Quayle, K. He, J. Shan, and K. Kash: MRS Commun. **3** (2013) 135. https://doi.org/10.1557/mrc.2013.19
9 A. Punya, W. R. L. Lambrecht, and S. M. Van: Phys. Rev. B **84** (2011) 165204. https://doi.org/10.1103/PhysRevB.84.165204
10 L. Han, K. Kash, and H. P. Zhao: J. Appl. Phys. **120** (2016) 103102. https://doi.org/10.1063/1.4962280
11 M. Rolles, B. Hyot B, and P. Miska: LED. Phys. Status. Solidi-R. **12** (2018) 1800173. https://doi.org/10.1002/pssr.201800173
12 M. R. Karim and H. P. Zhao: J. Appl. Phys. **124** (2018) 034303. https://doi.org/10.1063/1.5036949
13 A. Gorai and D. Biswas: Optik **158** (2017) 553. https://doi.org/10.1016/j.ijleo.2017.12.155
14 A. Gorai: Opt. Mater. **85** (2018) 337. https://doi.org/10.1016/j.optmat.2018.09.005
15 L. Lahourcade, N. C. Coronel, K. T. Delaney, S. K. Shukla, N. A. Spaldin, and H. A. Atwater: Adv. Mater. **25** (2013) 2562. https://doi.org/10.1002/adma.201204718
16 C. Wadia, A. P. Alivisatos, and D. M. Kammen: Environ. Sci. Technol. **43** (2009) 2072. https://doi.org/10.1021/es8019534
17 A. Laidouci, A. Aissat, and J. P.Vilcot: Sol. Energy **211** (2020) 237. https://doi.org/10.1016/j.solener.2020.09.025
18 D. V. Tim, F. Nathaniel, F. Q. Nicholas, M. L. Wojciech, O. S. David, F. J. P. Louis, and M. D. Steven: Solar Absorber. Ad. Energy Mater. **5** (2015) 1501462. https://doi.org/10.1002/aenm.201501462
19 X. Cao, F. Kawamura, Y. Ninomiya, T. Taniguchi, and N. Yamada: Sci. Rep. **7** (2017) 14987. https://doi.org/10.1038/s41598-017-14850-7
20 E. Arca, A. Fioretti, S. Lany, C. Adele, T. Glenn, C.Melamed, J. Pan, K. N. Wood, E.Toberer, and A. Zakutayev: IEEE J Photovolt. **8** (2018) 110. https://doi.org/10.1109/JPHOTOV.2017.2766522
21 N. Feldberg, J. D. Aldous, W. M. Linhart, L. J. Phillips, K. Durose, P. A. Stampe, R. J. Kennedy, D. O. Scanlon, G. Vardar, R. L. Field, T. Y. Jen, R. S. Goldman, T. D. Veal, and S. M. Durbin: Appl. Phys. Lett. **103** (2013) 042109. https://doi.org/10.1063/1.4816438
22 T. S. Wang and C. Y. Ni: Phys. Rev. B **95** (2017) 205205. https://doi.org/10.1103/PhysRevB.95.205205
23 H. Yıldırım: Phys. Lett. A. **383** (2019) 1324. https://doi.org/10.1016/j.physleta.2019.01.046
24 J. J. Shi and Z. Z. Gan: J. Appl. Phys. **94** (2003) 407. https://doi.org/10.1063/1.1576490
25 D. M. Zheng and Z. C. Wang: Commun. Theor. Phys. **58** (2012) 915.
26 D. M. Zheng, Z. C. Wang, and B. Q. Xiao: J. Semicond. **36** (2015) 033006. https://doi.org/10.1088/1674-4926/36/3/033006

27 N. S. Minimala, A. John Peter, and Y. C. K. Chang: Superlattice Microst. **60** (2013) 148. https://doi.org/10.1016/j.spmi.2013.04.017
28 W. M. Que: Phys. Rev. B. **45** (1992) 11036. https://doi.org/10.1103/PhysRevB.45.11036
29 S. Rudin and T. L. Reinecke: Superlattice Microst. **3** (1986) 137. https://doi.org/10.1016/0749-6036(87)90046-2
30 I. Vurgaftman, J. R. Meyer, and L. R. Ram-Mohan: J. Appl. Phys. **89** (2001) 5815. https://doi.org/10.1063/1.1368156
31 M. Suzuk, T. Uenoyama, and A. Yanase: Phys. Rev. B **52** (1995) 8132. https://doi.org/10.1103/PhysRevB.52.8132